This project has received funding from the European Union's Horizon 2020 research and innovation programme under grant agreement No 871813.

MUNDFAB

ICT Project No 871813

MUNDFAB

Modeling Unconventional Nanoscaled Device FABrication

D4.2: Report on the first round of optical and thermal measurements

P. Pichler (Fraunhofer), I. Bejenari (Fraunhofer), P. Evanschitzky (Fraunhofer), I. Deretzis (CNR), G. Mannino (CNR), A. Sciuto (CNR), A. La Magna (CNR), P. Michalowski (Łukasiewicz-IMiF), B. Sklenard (CEA), P. Acosta Alba (CEA), S. Kerdiles (CEA), A.S. Royet (CEA), F. Cristiano (CNRS)

March 31, 2021

Fraunhofer IISB leti cea tech cnrs Łukasiewicz Instytut Technologii Materiałów Elektronicznych life.augmented TU WIEN

Quality management
This deliverable was reviewed by:

Anne Hemeryck (LAAS-CNRS)

Eberhard Baer (Fraunhofer)

Contents

Executive Summary

This document reports on the first round of measurements for the determination of the optical properties of SiGe alloys with respect to temperature, alloy fraction and dopant concentration. SiGe alloys represent the most critical materials in terms of calibration for integration in Laser Annealing simulation tools, as previously reported in the MUNDFAB Deliverable 4.1 “Specification Report for Laser Annealing Calibration: Literature Review, Missing Data, Experimental Plan”. Measurements were performed for undoped and boron-doped crystalline blanket structures, as well as for pre-amorphized blanket structures. The data from the optical measurements were used to calibrate semiempirical formulas for the determination of the SiGe dielectric constants, which were subsequently integrated in laser annealing simulations of SiGe systems. This calibration was further validated by examining SIMS profiles of laser annealed SiGe structures. We notice that additional direct measurements of optical parameters will be integrated with the second set of microstructural characterizations and reported in the deliverable D4.7 “Complete model for alloy redistribution and doping calibrated with the second round of experiments”.

The document also presents a validation of the thermal properties of patterned systems by means of comparative electromagnetic wave simulations. This comparative analysis introduces benchmarks for the correct assessment of the absorption of electromagnetic waves during the process of laser annealing in complex geometries and for different materials used during the fabrication of microelectronic devices.

Due to the interrelationship of the treated topics, at least one representative of each partner has been involved in the preparation of derivable D4.2, whereas Fraunhofer has been tasked also with the organization of this derivable.

1. Introduction

Laser annealing (LA) with pulsed power emission (pulse duration below 10^{-6} s) can be integrated in thermal processes for micro-and nano-electronics, yielding versatile and powerful solutions in extremely constrained space and time scales (1) (2). Optimal control is a key issue for the successful application of LA during a thermal process flow. Due to the specificity of the electromagnetic energy absorption and the ultra-rapid thermal diffusion of the LA process, the potential benefits of LA require a complex process design, which is unique in microelectronics and overlaps with the device design. This complexity impacts on the Design of Experiments (DoE) for the optimization of LA processes. Within this context, reliable simulations of LA are required for optimizing the process parameters while reducing the number of experimental tests, with the help of a virtual DoE. The MUNDFAB project deals with the advanced TCAD of processes characterized by a low thermal budget, dedicating WP4 to the simulation of laser annealing. Among the various issues considered in WP4, a critical one is the calibration of material parameters, which is fundamental for allowing the full predictivity of the models. In derivable D4.1, a systematic categorization of the physical parameters required for the successful simulation of LA processes has been reported for several materials used in microelectronic devices. Critical issues with respect to parameter calibration were also identified, with SiGe alloys showing a high level of criticality due to the non-definite nature of their lattice and the dependence of the optical parameters on the alloy fraction and dopant concentration. D4.2 reports on experimental measurements that have been performed in order to extract the optical constants of SiGe under different temperatures, stoichiometries and dopant concentrations. These results have been used for the derivation and calibration of semiempirical functions that can be used within the LA simulation workflow. Based on this scheme, LA process simulations were performed by existing custom research tools at the CNR and CEA. Results were readily compared with experimental SIMS measurements of similar structures and processes.

In addition to parameter calibration for SiGe alloys, the reliability of LA process simulations has been further validated by means of electromagnetic wave (EMW) calculations, which are fundamental for the modelling of heating in microelectronic devices. EMW computations were performed in custom research tools at the CNR using quasi-adiabatic methods, which integrate the power release over many oscillations of the EMWs (2). These calculations were compared with simulations of power dissipation in nano-structured topographies based on an accurate and specialized tool developed in the Fraunhofer institute (Dr.LiTHO) (3). Results have corroborated the quasi-adiabatic approach and its use in the modelling of laser annealing.

2. DoE of the optical measurements in SiGe samples

Based on the DoE presented in derivable D4.1, the first batch of samples for the direct optical measurements has been fabricated by the CEA-LETI. They were a set of strained SiGe undoped 30nm thick films over a Si substrate (obtained from epitaxial growths below the critical thickness) with 10%, 20%, 30%, and 40% Ge content, and a set of p-doped (with boron) strained SiGe samples with 30% Ge content. The Ge profiles have been measured in Ł-IMiF by means of Secondary Ions Mass Spectroscopy (SIMS) and the measured B concentrations were: 7.3×10^{19} (Low), 1.4×10^{20} (Medium) 2.3×10^{20} cm^{-3} (High). A “very low doped” sample was also fabricated in a second batch, with a B concentration of ~5×10^{18} cm^{-3}. Moreover, two pre-amorphized (PAI) blanket samples were fabricated with 30% of Ge content: an undoped and

a Low-doped one. All samples were delivered to the CNR for the determination of their optical properties by means of spectroscopic ellipsometry.

3. Spectroscopic ellipsometry for SiGe

The spectroscopic analysis of the optical properties in the fabricated SiGe samples was performed with a J. A. Woollam VASE Ellipsometer. The system had a vertical configuration, and it was equipped with an autoretarder tool. The light source was composed of a Xe lamp and a monochromator. Wavelength-by-wavelength measurements were performed at variable temperatures [starting from room temperature (RT) up to 600 °C], mounting an Instec closed chamber with an overpressure of N_2 gas. The presence of the monochromator was particularly important, as it allowed for an optimized measurement step in specific spectral regions (i.e., a wavelength step of 0.5 nm in the range 300-320 nm, corresponding to a photon energy step of 0.007 eV in the range 4.13-3.87 eV) which are relevant for laser annealing processes. A wider step was used elsewhere within the range 1-6 eV.

We initially estimated the layer thickness for all samples in the transparent region, using Cauchy's formula. The thickness was found to be ~30 nm, as expected from the specification of the grown samples. By fixing the thickness parameter, the dielectric function was obtained by fitting experimental data with the Tauc-Lorentz dispersion formula (4) using four oscillators. Apart from the parameters used for each oscillator, we have also evaluated two additional properties of the samples: the Ge content and the surface roughness. The Ge content corresponded very well to the nominal content (in the whole range 10-40%), whereas the surface roughness was found to be 2 nm on average for all samples. Initial measurements took place at room temperature. Figure 1a shows the real and imaginary part of the dielectric function of the SiGe samples as a function of the photon energy for different Ge contents (including also the case of bulk Si) and doping concentrations.

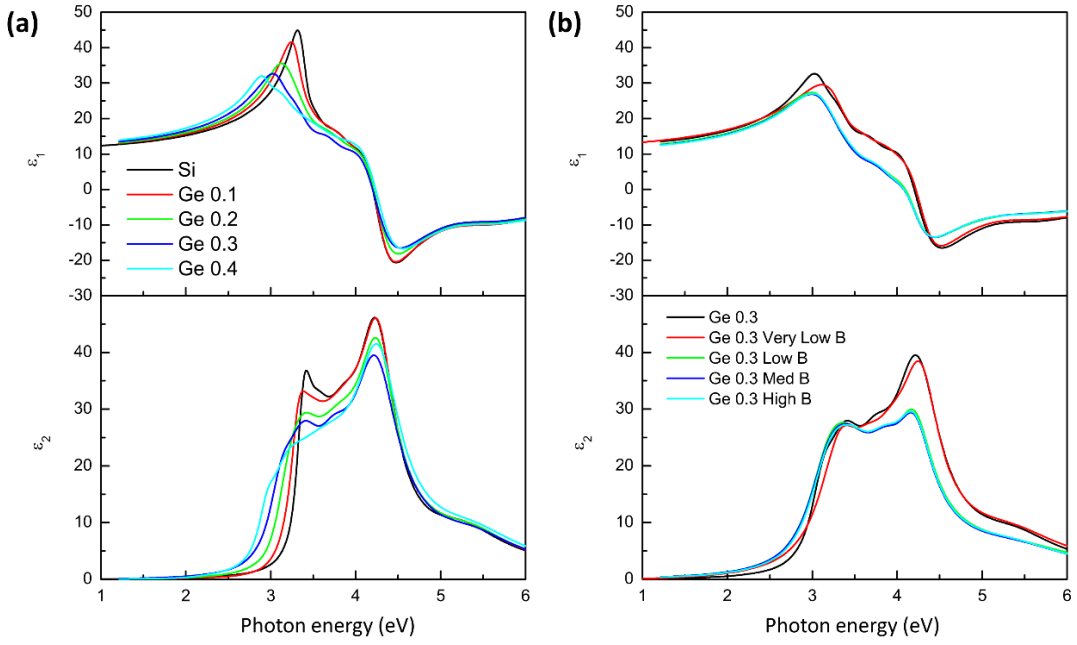

Figure 1: Real (ε_1) and imaginary (ε_2) part of the dielectric function with respect to the photon energy at room temperature for (a) undoped SiGe samples with variable Ge alloy fraction (from 10-40%) and (b) fixed 30% Ge content and variable doping concentrations.

The 30% alloy fraction of Ge was chosen to fabricate doped samples having three distinct dopant concentrations (Low, Medium, High), as described in paragraph 2. However, the dielectric function did not differ significantly in the three cases (see Figure 1b). The dielectric function of the “very low doped” sample was instead closer to the undoped case, indicating that the dependence of the optical constants from the doping concentration is not linear and saturates for doping levels higher than ~7×10^{19} cm^{-3} (Figure 1b).

We then performed temperature-dependent measurements for the four SiGe undoped samples at three different constant temperatures (200°C, 400°C, 600°C), to estimate the value of the dielectric function during laser irradiation (see Figure 2a), as the latter induces heating. The trend of these measurements was similar for all Ge contents, with a redshift of the absorption spectrum (see ε_2) when increasing the temperature. The three doped samples instead showed similar curves for all annealing temperatures, having however significant differences with respect to the non-annealed case for energies above ~3.3 eV (see Figure 2b).

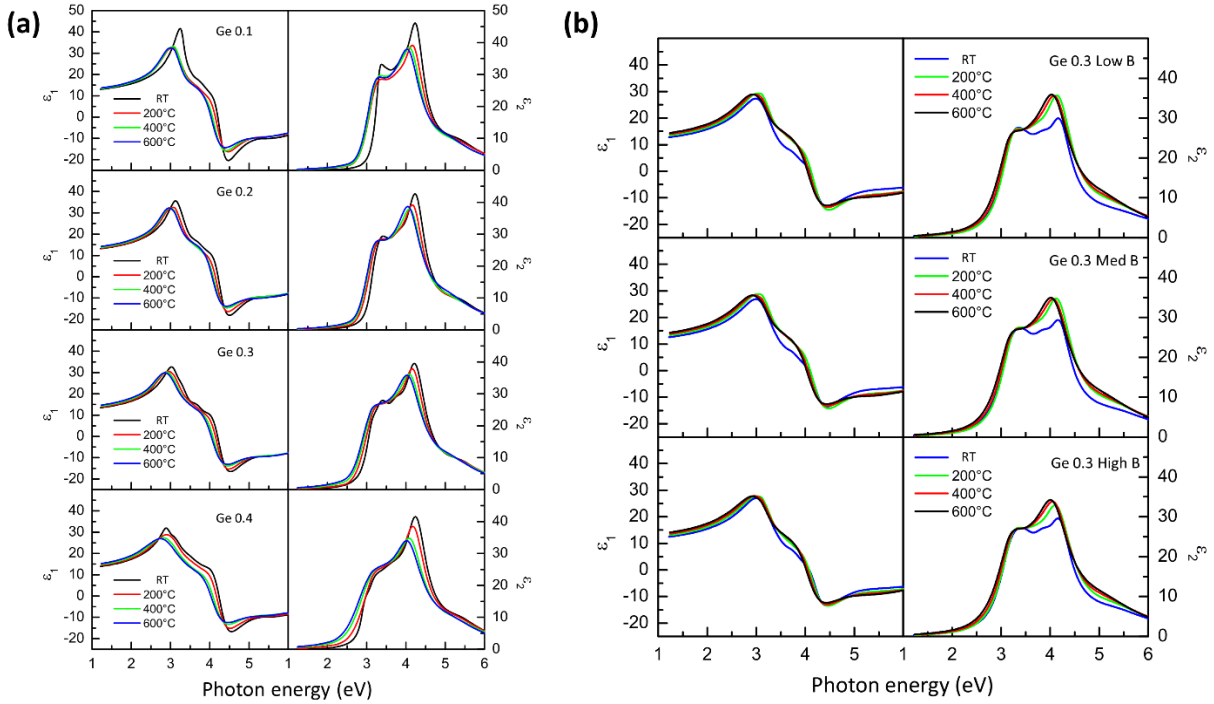

Figure 2: Real (ε_1) and imaginary (ε_2) part of the dielectric function with respect to the photon energy for SiGe samples at different temperatures. (a) Undoped samples with variable Ge alloy fraction (from 10-40%). (b) Samples with a fixed Ge alloy fraction (30%) and variable doping concentrations.

In the second batch of samples, we have also analysed two pre-amorphized samples: an undoped sample and a Low-doped sample. In both cases, a 30% Ge content was chosen for the alloy stoichiometry. The dielectric function reported in Figure 3a was very smooth for both amorphized samples and differed substantially from the peaked curves observed for the crystalline materials.

We finally performed ellipsometric measurements on the PAI samples during isothermal cycles at increasing temperatures, as shown in the top frame of Figure 3b. The samples were kept at each temperature for 25 min, during which we performed the measurements. We note that these measurements were very sensitive in revealing a continuous but relatively small variation of the optical constants from 100 °C up to 500 °C. At 550 °C instead, a sudden variation of the

dielectric function occurred, due the early nucleation and growth of crystal gains inside the amorphous matrix. However, most part of the layer preserved the amorphous characteristics at this temperature. At 600 °C we observed a further conversion of the dielectric constants towards those of the fully crystalline phase. However, a complete amorphous-to-crystalline conversion was not achieved, even after a second annealing process. The 600 °C temperature represents the instrumental limit of the stage, excluding measurements at higher temperatures.

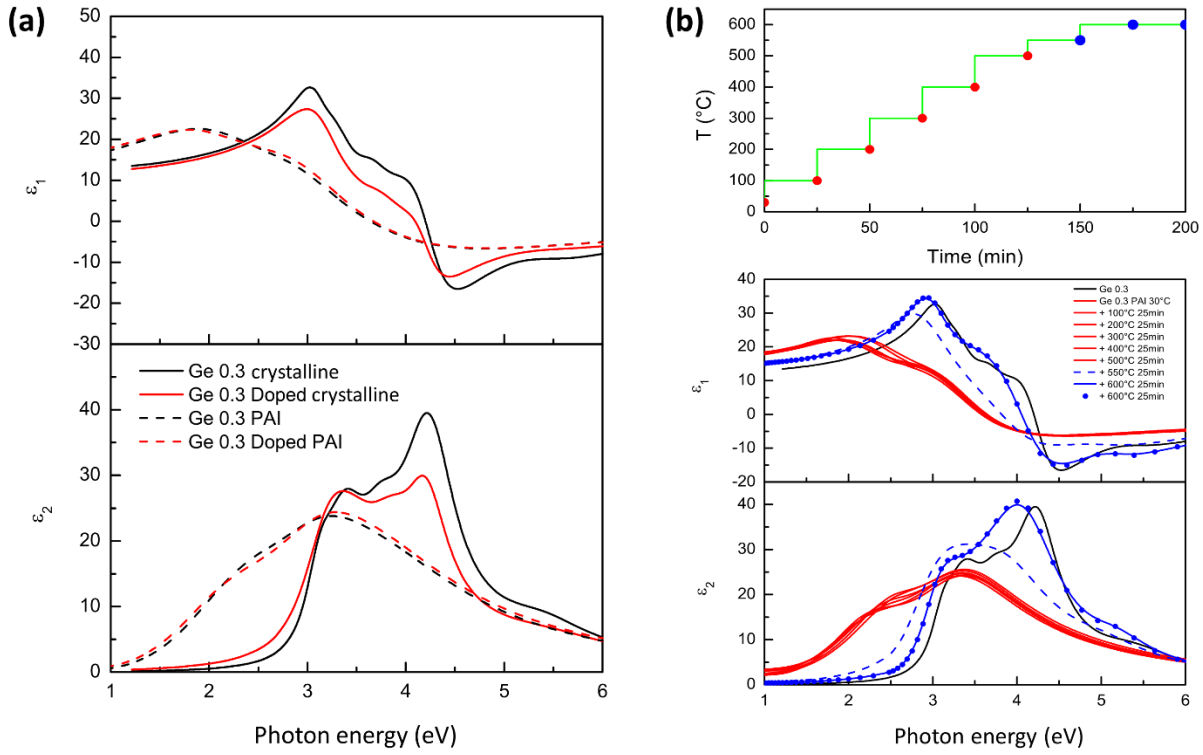

Figure 3: (a) Real (ε_1) and imaginary (ε_2) part of the dielectric function with respect to the photon energy for an undoped and a Low-doped pre-amorphized (PAI) $Si_{0.7}Ge_{0.3}$ sample. The respective crystalline curves are shown for comparison (full lines). (b) Scheme of the ellipsometric measurements for PAI samples during isothermal cycles at increasing temperatures (upper). Real (ε_1) and imaginary (ε_2) part of the dielectric function for an undoped PAI $Si_{0.7}Ge_{0.3}$ sample upon isothermal annealing from RT to 600 °C.

4. Updated calibration of the optical constants in SiGe

In the MUNDFAB Deliverable 4.1 “Specification Report for Laser Annealing Calibration: Literature Review, Missing Data, Experimental Plan” a set of calibrated parameters has been presented for the optical and thermal properties of several materials of interest for laser annealing processes. In that report, some critical issues were identified, with SiGe being a main concern due to its alloy composition and the variation of its optical characteristics based on the alloy fraction, dopant concentration and temperature. Considering the importance of SiGe in future microelectronic devices, a new calibration of the optical constants for SiGe is proposed here, based on the ellipsometric measurements presented in the previous paragraph. The calibration is structured on the basis of the following theoretical scheme:

SiGe is an almost ideal binary alloy system, where Si and Ge are fully miscible in the whole range of composition. This fact generally makes the linear interpolation between the physical properties of Si and Ge (using the Ge alloy fraction variable X) a good starting point for the calibration of this material (5). However, some critical uncertainties exist. A more accurate

determination of the dependence of the optical parameters on X in each phase is necessary. Moreover, the dependence of the parameters in the disordered phases (liquid and amorphous) on X is barely determined by direct measurements: The usual approach here is to use the same relations as for the crystalline phase. We express the optical parameter P (e.g., the real or the imaginary part of the dielectric function) as:

$$P_{SiGe}(T,X) = P_{Ge}(T) \times f^n_P(X,T) + P_{Si}(T) \times [1 - f^n_P(X,T)]$$

where $f^n_P(X,T)$ is monotonically growing polynomial function of degree *n* satisfying the obvious relationships $f^n_P(0,T) = 0$, $f^n_P(1,T)=1$ while $P_{Ge}(T)$ and $P_{Si}(T)$ are the Ge and Si parameters reported in the Tables 1-6 of Derivable D4.1. Therefore, only $f^n_P(X,T)$ has an unknown form and calibration. If we consider a second order polynomial function $f^2_P(X,T)$, we have:

$$f^2_P(X,T) = a(T) \times X^2 + [1 - a(T)] \times X$$

We note here that such a function fulfils the $f^2_P(0,T) = 0$, $f^2_P(1,T)=1$ constraints that reflect the limiting conditions where the content of Ge is either 0% (pure Silicon) or 100% (pure Germanium). In order to consider the temperature dependence of the optical constants, function a(T) has been further calibrated as a second-order unrestricted polynomial function:

$$a(T) = b \times T^2 + c \times T + d,$$

where b, c and d represent the calibrated parameters from the experimental measurements. A second level of calibration is necessary when SiGe samples are doped. In this case, a function $E_{SiGe}(T,X,C)$ can be introduced, where C represents the dopant concentration in the samples:

$$E_{SiGe}(T,X,C) = P_{SiGe}(T,X) \times g(C,T)$$

where $g(C,T) = 1 - m(T) \times C/C_0$. Here, $m(T) = b' \times T^2 + c' \times T + d'$ is an unrestricted second-order polynomial function of temperature with parameters b', c' and d', while C_0 is a constant that allows for $g(C,T) \approx 1$ in the case of very low-doping (hence, for very low doping, $E_{SiGe}(T,X,C) \approx P_{SiGe}(T,X)$). The full parametrization and optical constant calibration for wavelength λ=308 nm (corresponding to the used laser line during laser annealing experiments) is reported in Table 1. We note that the expressions for crystalline Si and Ge are obtained from in-house parameterizations and from Ref. (6).

Parameter	Description	Values related to Real Permittivity (ε1)	Values related to Imaginary Permittivity (ε2)
$P_{Ge}(T)$	Permittivity function for Ge	3.91230E-06*T^2 - 1.35530E-02*T + 8.94077	-5.22533E-06*T^2 + 1.59269E-02*T + 23.5712
$P_{Si}(T)$	Permittivity function for Si	-9.025E-7* T^2 - 6.55813E-3*T + 13.8925	9.652E-3* T + 35.0688
b	Parameter for function a(T)	2.69960559E-06	6.16719594E-07
c	Parameter for function a(T)	-8.93283612E-03	-3.76779637E-03
d	Parameter for function a(T)	2.74738922E+00	7.24082338E-01
b'	Parameter for function m(T)	-3.04319581E-08	-1.55547589E-09
c'	Parameter for function m(T)	8.79752533E-05	5.51655818E-07
d'	Parameter for function m(T)	-4.73111366E-03	4.13092579E-03
C_0	Constant for function g(C,T)	1.00E+19	1.00E+19

Table 1: Calibrated parameters and base functions for the real and imaginary permittivity of SiGe alloys which allow one to describe these permittivities as a function of temperature, alloy fraction and boron doping concentration. The calibration has been performed considering optical data with a wavelength of 308 nm. The unit of temperature in P_{Ge} and P_{Si} is Kelvin whereas the unit of C_0 is cm^{-3}.

Figure 4 shows the calculated reflectivity for undoped (**a**) and boron-doped (**b**) samples, based on the real and imaginary dielectric functions of our theoretical scheme. In Figure 4a, we note that calibration for undoped samples took place for different Ge contents (see paragraph 2), also including the cases of pure silicon and pure germanium at room temperature (as limit cases). The calibration in Figure 4b (regarding boron-doped samples) was instead based on a single Ge content (30%) and different dopant concentrations. Further improvements in the calibration will be pursued during the project, upon additional availability of experimental data.

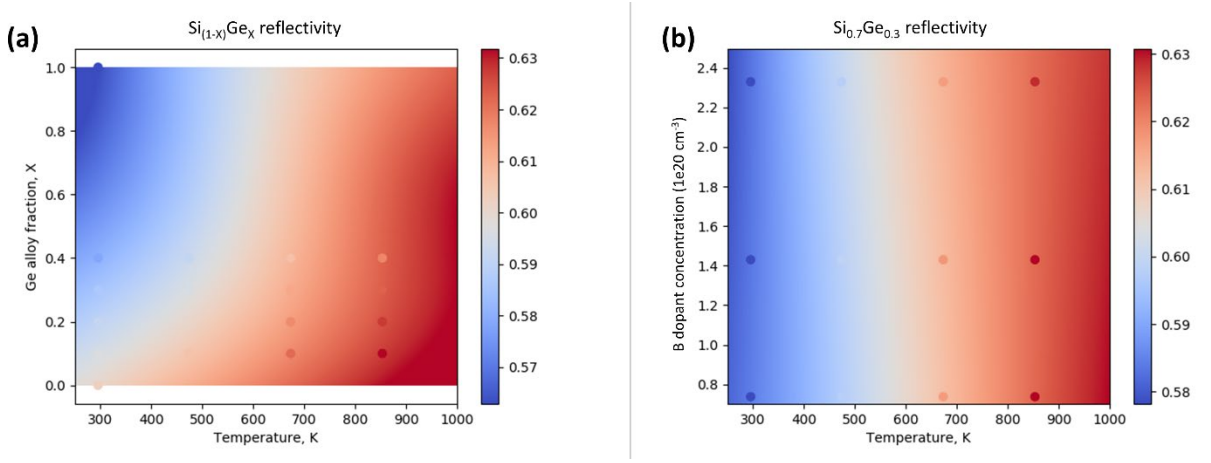

Figure 4: (a) Calibrated reflectivity for undoped SiGe samples as a function of the Ge alloy fraction and the temperature. (b) Calibrated reflectivity for B-doped $Si_{0.7}Ge_{0.3}$ samples as a function of the dopant concentration and the temperature. The colour-scale indicates the value of the reflectivity. Coloured dots represent the experimental values. A 308 nm photon wavelength was considered for both experimental and theoretical results.

Finally, to make uniform the calibration scheme beyond the dielectric permittivity, we have defined all other SiGe parameters of interest for LA simulations (see derivable D4.1) as a linear interpolation of the respective values for pure silicon and germanium, on the basis of their percentage within the SiGe alloy.

5. SiGe laser annealing modelling and experimental validation through SIMS

An early evaluation of the proposed calibrated scheme for SiGe has been performed at the CNR and CEA by simulating laser annealing processes with the aid of custom research software. These simulations targeted in replicating equivalent experimental processes for Low-doped blanket $Si_{0.7}Ge_{0.3}$ samples irradiated with the pulsed excimer laser annealing system of CEA-LETI. The laser line had a 308 nm wavelength and a 160 ns pulse duration, while irradiation took place on 15 × 15 mm^2 areas. We note that the LA code can dynamically load pre-annealing profiles for Si, Ge and the dopant, following their time evolution for the entire annealing process. Both simulations and experiments regard a single pulse annealing process. We set the total time duration of the simulation at 400 ns for three different laser fluences (1.6 J/cm^2, 1.95 J/cm^2 and 2.2 J/cm^2): no significant evolution of the alloy fraction and dopant field occurs after this time step. We note that this energy range is suitable for a wide range of regimes and melting depths. Comparative results for the concentration of Ge throughout the sample depth can be seen in Figure 5. We notice an overall good agreement of the simulated and the experimental profiles, particularly for the case of the lower laser fluence, where a partial-melt regime close to the sample surface can be observed. Increasing the laser fluence expands the melt area, while a full melt regime can be simulated for a fluence of 2.2 J/cm^2. We

point out that random sites of the melting nucleation and the liquid-solid interface roughness will be better discussed in Deliverable 4.3 entitled “First round of experiments on structural modifications, alloy redistribution to validate model predictions, experimental plan for second round”. There, a better description of some quantitative differences between the SIMS profiles (which are integrated over a relatively large area) and strictly 1D simulations will be presented.

Further efforts will be dedicated for the improvement of the calibration in LA simulations during the MUNDFAB project, particularly focusing on the more accurate calibration of the self-consistent features regarding the evolving fields of dopant atom density and alloy fraction in the liquid phase. Additional developments and comparisons between simulated and experimental results will be presented in the Deliverable D4.4 entitled “Beta version of the laser-annealing models implementing a complete calibration of the optical and thermal properties for all the device materials”.

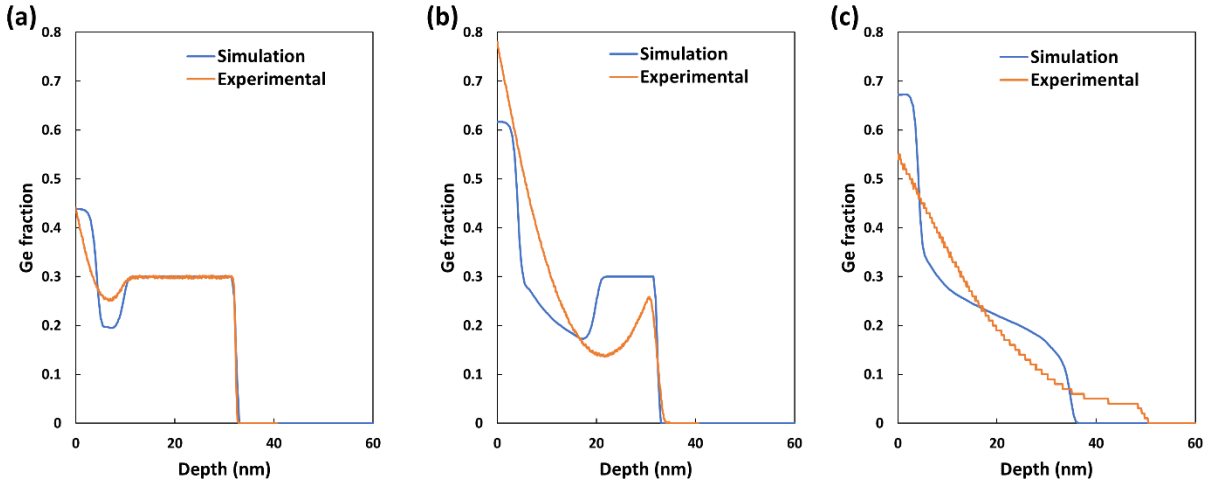

Figure 5: Simulation of laser annealing processes for a $Si_{0.7}Ge_{0.3}$ sample (blue lines) and comparison with experimental SIMS profiles (orange lines), considering three different laser fluences: (a) 1.6 J/cm^2, (b) 1.95 J/cm^2 and (c) 2.2 J/cm^2. The initial Ge profile had a constant value of 0.3 over the entire SiGe sample depth (~32nm).

6. Benchmark of heat source calculations in patterned structures

The proper description of heating in laser annealing models represents one of the key issues for the reliable simulation of actual processes. In the custom tools owned by the CNR and CEA, heating is modelled as the time harmonic solution of Maxwell’s equations, where the laser heat source *S(**r**,t)* is described as:

$$S(\boldsymbol{r},t) = \frac{\epsilon_2}{2\varrho}|\boldsymbol{E}_{t-h}|^2$$

Here, ϵ_2 is the imaginary part of the complex dielectric function of the heated material, $\boldsymbol{E}_{t-h}$ is the time harmonic electric field and $|\boldsymbol{E}_{t-h}|^2$ represents the intensity of the electromagnetic field. To validate the accuracy of this approach, we have compared the results of heating source distribution in complex SiGe structures obtained from these custom tools, with EMW calculations based on the Dr. LiTHO software (3). The latter accurately estimates the dissipation of electromagnetic energy in these complex geometries, based on the finite-difference time-domain and the waveguide methods. The two quantities that have been evaluated are the spatial distribution of the intensity of the electromagnetic waves and their

absorption (which is proportional to the heat generation density) within the irradiated materials. Figure 6 shows a simple geometry of the $Si_{0.9}Ge_{0.1}$ periodic FinFET structure (considering periodic boundary conditions at the left and right borders) on a silicon substrate. Results for both intensity and absorption of the electromagnetic waves are in very good agreement, indicating that the quasi-adiabatic approach of the custom laser annealing solvers can adequately simulate the heating process. An important issue is the verification of this electromagnetic congruency also for temperatures above RT, as the laser process itself should induce heating up to melting temperatures, which is necessary for the activation of dopants. Figure 7 shows the comparison of results between the two methods for a $Si_{0.8}Ge_{0.2}$ FinFET structure at three different constant temperatures (300 K, 873 K, 1273 K). Also here, the agreement between the two theoretical schemes is evident, with the electromagnetic intensity showing two maxima at the lateral edges of the FinFET at 300 K, which tend to merge for higher temperatures. Finally, we have evaluated the compatibility of the two approaches for geometries with a higher level of complexity, regarding an over-etched FinFET structure (Figure 8) and a SiGe trench with an oxide mask on top (Figure 9). We note that for the trench structure, a clear difference in the EMW intensity can be observed in the oxide and SiGe parts of the layer. Results were satisfactory even for these complex-geometry structures, further validating the quasi-adiabatic approach for heating in laser annealing simulations. Based on the above results, a decision to continue the simulation campaign with the quasi-adiabatic model of the custom laser annealing tools was taken.

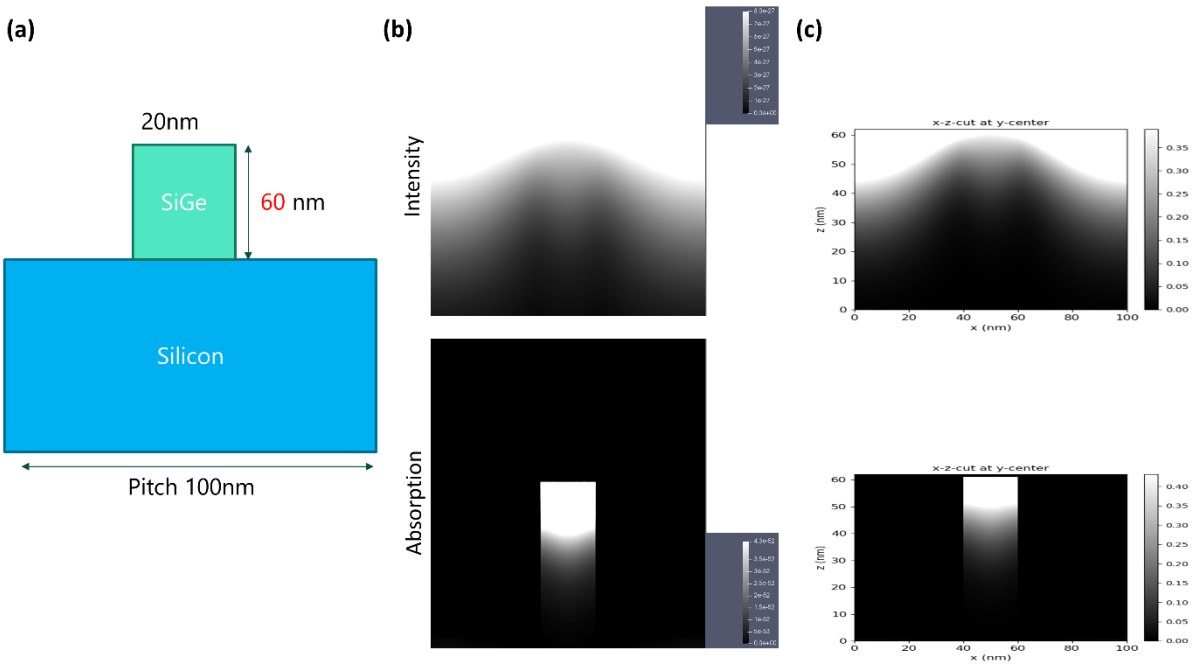

Figure 6: (a) FinFET structure based on $Si_{0.9}Ge_{0.1}$ with a width of 20 nm and a height of 60 nm on a silicon substrate with a pitch of 100 nm. (b) Calculations of the spatial distribution of the intensity of the electromagnetic field (upper) and its absorption by the $Si_{0.9}Ge_{0.1}$ material (lower) at 300 K, based on custom research tools at the CNR using quasi-adiabatic methods. (c) Similar calculations as in (b) based on power dissipation, using the Dr. Litho software. The different numerical scales between the two software are due to different normalization conditions.

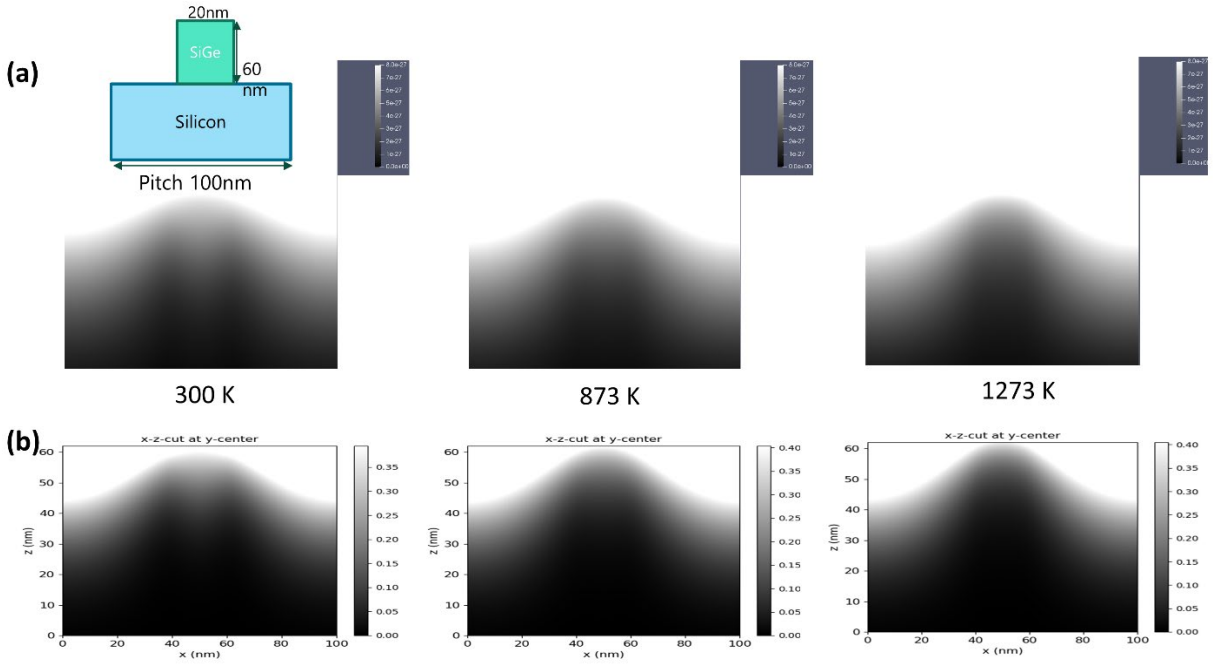

Figure 7: Comparison between the spatial distribution of electromagnetic wave intensity for different temperatures based on custom research tools at the CNR (a) and the Dr. Litho software (b). The target structure is a FinFET based on $Si_{0.8}Ge_{0.2}$ with a width of 20 nm and a height of 60 nm on a silicon substrate with a pitch of 100 nm.

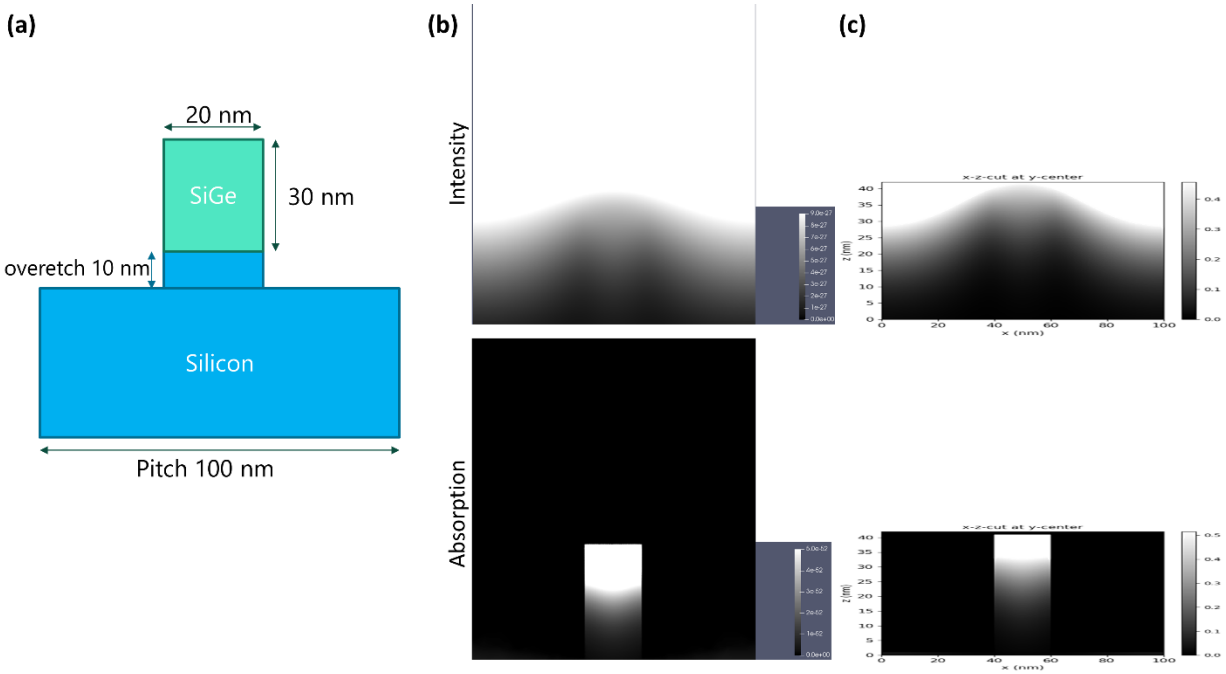

Figure 8: (a) Overetched FinFET structure based on $Si_{0.9}Ge_{0.1}$ with a width of 20 nm and a height of 30 nm on a 10-nm-high silicon etching, on top of a silicon substrate with a pitch of 100 nm. (b) Calculations of the spatial distribution of the intensity of the electromagnetic field (upper) and its absorption by the $Si_{0.9}Ge_{0.1}$-Si material (lower) at 300 K, based on custom research tools at the CNR using quasi-adiabatic methods. (c) Similar calculations as in (b) based on power dissipation, using the Dr. Litho software.

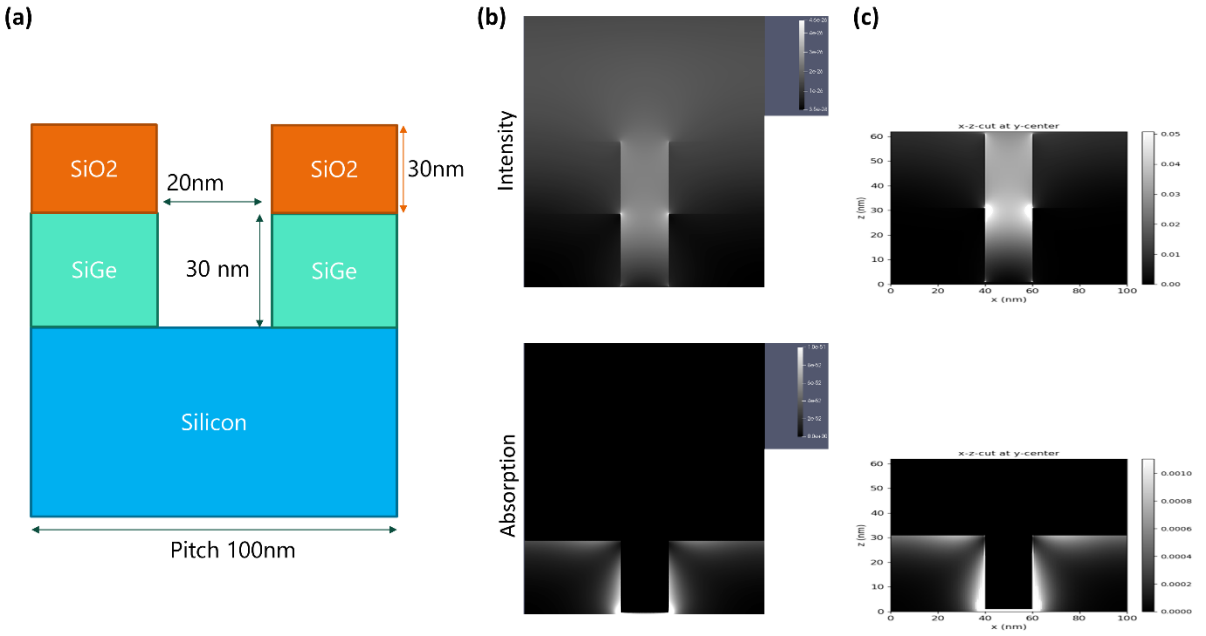

Figure 9: (a) $Si_{0.9}Ge_{0.1}$ trench structure having an oxide mask with a width of 20 nm and a height of 30 nm on a silicon substrate with a pitch of 100 nm. (b) Calculations of the spatial distribution of the intensity of the electromagnetic field (upper) and its absorption by the SiO_2 and $Si_{0.9}Ge_{0.1}$ materials (lower) at 300 K, based on custom research tools at the CNR using quasi-adiabatic methods. (c) Similar calculations as in (b) based on power dissipation, using the Dr. Litho software.

7. Conclusions

In this deliverable we have provided the direct (optical) measurements and experiments for crystalline and pre-amorphized SiGe alloys, which have been used to introduce improved calibrated models for laser annealing simulations. We will use these models “ex ante” for any evaluation of LA processes in the MUNDFAB project. We have moreover assessed the heating module of the LA simulation scheme through comparative electromagnetic wave calculations in complex device geometries, using standard tools for LA modelling along with accurate dissipative methods based on a rigorous simulation of light/matter interaction. Deliverable D4.2, in conjunction with Deliverable D4.1, represents the cornerstone for the calibration/evaluation of continuous LA models, while it constitutes the basis for the advanced LA modelling schemes that will be pursued during the rest of the project.

References

1. **A. La Magna, P. Alippi, V. Privitera, G. Fortunato, M. Camalleri, B. Svensson.** A phase-field approach to the simulation of the excimer laser annealing process in Si. *Journal of Applied Physics.* AIP, 2004, Vol. 95, 9, p. 4806.

2. **S.F. Lombardo, G. Fisicaro, I. Deretzis, A. La Magna, B. Curver, B. Lespinasse, K. Huet.** Theoretical study of the laser annealing process in FinFET structures. *Applied Surface Science.* Elsevier, 2019, Vol. 467–468, 666-672.

3. *Dr.LiTHO – A Development and Research Lithography Simulator.* **Tim F¨uhner, Thomas Schnattinger, Gheorghe Ardelean, and Andreas Erdmann.** Proc. SPIE 6520, Optical Microlithography XX, 65203F : International Society for Optics and Photonics, 2007. DOI: 10.1117/12.709535.

4. **G. E. Jellison Jr., F. A. Modine.** Parameterization of the optical functions of amorphous materials in the interband region. *Appl. Phys. Lett.* 1996, Vol. 69, 371.

5. **F., Schaffler.** *in "Properties of Advanced SemiconductorMaterials GaN, AlN, InN, BN, SiC, SiGe".* New York : Eds. Levinshtein M.E., Rumyantsev S.L., Shur M.S., John Wiley & Sons, Inc., 2001. p. 149-188.

6. **K. Huet, J. Aubin, P.-E. Raynal, B. Curvers, A. Verstraete, B. Lespinasse, F. Mazzamuto, A. Sciuto, S.F. Lombardo, A. La Magna, P. Acosta-Alba, L. Dagault, C. Licitra, J.-M. Hartmann, S. Kerdilès.** Pulsed laser annealing for advanced technology nodes: Modeling and calibration. *Applied Surface Science.* Elsevier, 2020, Vol. 505, 144470.